Angewandte Chemie

GDCh

Eine Zeitschrift der Gesellschaft Deutscher Chemiker

www.angewandte.de

2018–130/10

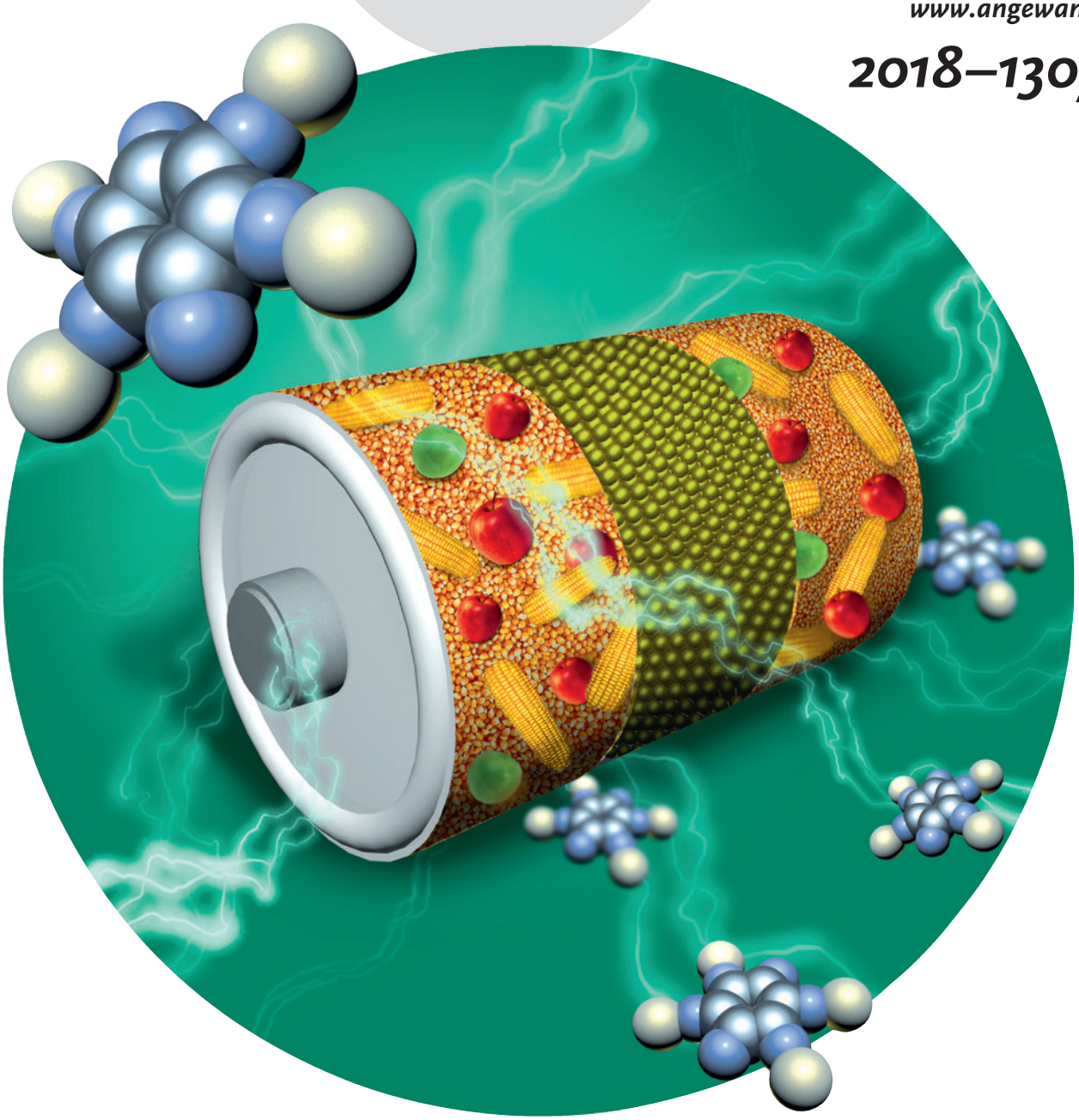

Titelbild

Y. Yao et al.

Tailored Organic Electrode Material Compatible with Sulfide Electrolyte for Stable All-Solid-State Sodium Batteries

ANCEAD 130 (10) 2531–2776 (2018) · ISSN 0044–8249 · Vol. 130 · No. 10

WILEY-VCH

Energy Storage Materials

Deutsche Ausgabe: DOI: 10.1002/ange.201712895
Internationale Ausgabe: DOI: 10.1002/anie.201712895

Tailored Organic Electrode Material Compatible with Sulfide Electrolyte for Stable All-Solid-State Sodium Batteries

*Xiaowei Chi[+], Yanliang Liang[+], Fang Hao, Ye Zhang, Justin Whiteley, Hui Dong, Pu Hu, Sehee Lee, and Yan Yao**

Abstract: *All-solid-state sodium batteries (ASSSBs) with nonflammable electrolytes and ubiquitous sodium resource are a promising solution to the safety and cost concerns for lithium-ion batteries. However, the intrinsic mismatch between low anodic decomposition potential of superionic sulfide electrolytes and high operating potentials of sodium-ion cathodes leads to a volatile cathode–electrolyte interface and undesirable cell performance. Here we report a high-capacity organic cathode, $Na_4C_6O_6$, that is chemically and electrochemically compatible with sulfide electrolytes. A bulk-type ASSSB shows high specific capacity (184 mAh g^{-1}) and one of the highest specific energies (395 Wh kg^{-1}) among intercalation compound-based ASSSBs. The capacity retentions of 76% after 100 cycles at 0.1 C and 70% after 400 cycles at 0.2 C represent the record stability for ASSSBs. Additionally, $Na_4C_6O_6$ functions as a capable anode material, enabling a symmetric all-organic ASSSB with $Na_4C_6O_6$ as both cathode and anode materials.*

In contrast to traditional liquid batteries, all-solid-state batteries use non-flammable, thermally and mechanically stable solid-state electrolytes (SSEs) that could potentially block metal dendrites and enable direct-series-stacking of individual cells, therefore offering better safety and potentially higher energy density.[1] For large-scale energy storage, all-solid-state sodium batteries (ASSSBs) are especially attractive thanks to the vast abundance of sodium element on the Earth. Table S1 in the Supporting Information summarizes all reported ASSSBs with key performance parameters. ASSSBs using oxide electrolytes show low reversible capacity and fast capacity decay (< 60% retention in 10 cycles) due to poor contact at the cathode–electrolyte interface,[2] while those with polymer electrolytes show large polarization and low active material utilization as the result of low ionic conductivity.[3] Sulfide SSEs feature superior formability and high Na-ion conductivities,[4] but have challenges in their narrow electrochemical stability window.[5] The anodic decomposition potential is reported to be as low as 2.3 V (theoretical)/2.7 V (experimental) versus Na^+/Na for the representative electrolyte Na_3PS_4.[5b] This potential is well below the operating potential of most intercalation-type cathode materials previously reported for ASSSBs such as $NaFePO_4$,[2a] $Na_3V_2(PO_4)_3$,[2b] $Na_{2/3}Co_{2/3}Mn_{1/3}O_2$,[3a] and $NaCrO_2$[6] (Figure 1). The chemical reactions between sulfide electrolytes and cathode materials result in resistive interfacial layers that deteriorate cell performance.[5b,6–7] Such electrochemical and chemical incompatibility in all-solid-state lithium batteries (ASSLBs) can be alleviated by precoating cathode materials with inert Li-ion conductors ($LiNbO_3$, Li_3PO_4, etc.).[8] The Na-ion-conducting counterpart of coating materials have been theoretically predicted only recently[9] and are yet to be implemented experimentally. Cathode materials with lower operating potentials such as TiS_2 suffer from intrinsically low reaction reversibility.[5a,10] Conversion-type cathode materials such as S and Na_2S operate at sufficiently low potentials, but it remains challenging to manage the large volume change during cycling.[11] Therefore, new Na-intercalation cathode materials with chemical and electrochemical compatibility with sulfide electrolytes are necessary for building high-performance sulfide-based ASSSBs.

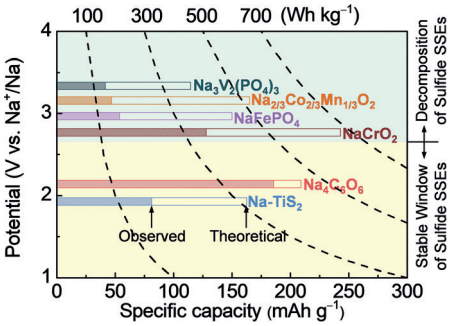

Figure 1. Potential–capacity plot for previously reported intercalation-type cathode materials and $Na_4C_6O_6$ for ASSSBs. Shadow and blank bars represent the observed and theoretical specific capacities, respectively. Specific energy is calculated considering a sodium anode.

Organic carbonyl compounds (OCCs) with controllable molecular design and sustainable resource are promising electrode materials.[12] Most OCCs operate within 1.5–2.5 V versus Na^+/Na,[12b] which falls within the stable window of sulfide SSEs (yellow region of Figure 1). OCCs also deliver

[*] Dr. X. W. Chi,[+] Dr. Y. L. Liang,[+] F. Hao, Y. Zhang, H. Dong, Dr. P. Hu, Prof. Y. Yao
Department of Electrical and Computer Engineering and Materials Science and Engineering Program
University of Houston, Houston, TX 77204 (USA)
E-mail: yyao4@uh.edu
Dr. J. Whiteley, Prof. S. Lee
Department of Mechanical Engineering
University of Colorado at Boulder
Boulder, CO 80309 (USA)
[+] These authors contributed equally to this work.
Supporting information and the ORCID identification number(s) for the author(s) of this article can be found under: https://doi.org/10.1002/anie.201712895.

 © 2018 Wiley-VCH Verlag GmbH & Co. KGaA, Weinheim

much higher specific capacities (200–500 mAh g^{-1}) than previously reported sodium intercalation cathode materials (100–200 mAh g^{-1}).[12a,13] Therefore, we expect OCCs to avoid the aforementioned incompatibility issues but still deliver competitive specific energy. Herein we report for the first time on a tailored OCC, $Na_4C_6O_6$, with an average voltage of 2.15 V versus Na^+/Na and a theoretical specific capacity of 205 mAh g^{-1} based on a two-electron two-sodium reaction between $Na_4C_6O_6$ and $Na_2C_6O_6$. ASSSBs were built using Na_3PS_4 SSE[10a] which has a Na-ion conductivity of $> 10^{-4}$ S cm at room temperature and an anodic decomposition potential of 2.7 V versus Na^+/Na. Both the chemical and electrochemical compatibilities between $Na_4C_6O_6$ and Na_3PS_4 were investigated. Furthermore, $Na_4C_6O_6$ can also function as a capable anode material with a high theoretical specific capacity of 205 mAh g^{-1} based on a two-electron two-sodium reaction between $Na_4C_6O_6$ and $Na_6C_6O_6$, adding to the limited choices of anode materials for sulfide-based ASSSBs where only NaSn alloys ($Na_{15}Sn_4$, Na_2Sn, etc.) are known to work to certain degree.[5b,10a] We have demonstrated a symmetric all-organic $Na_4C_6O_6$/Na_3PS_4/$Na_4C_6O_6$ full cell.

$Na_4C_6O_6$ was synthesized from commercially available $Na_2C_6O_6$ (*comm*-$Na_2C_6O_6$) by reduction with sodium naphthalenide ($NaC_{10}H_8$) in tetrahydrofuran (THF) (Figure 2a). The molar ratio of $NaC_{10}H_8$ to $Na_2C_6O_6$ is the stoichiometric 2:1. Pristine *comm*-$Na_2C_6O_6$ has a particle size of ca. 50 μm in diameter (Figure 2b), which was ball-milled to less than 1 μm to facilitate reduction. Subsequent reduction further downsized $Na_4C_6O_6$ to nanoparticles (200–300 nm). The small particle size will increase the contact area between electrolyte and electrode particle and facilitate charge transfer.[14] The thermal stability of the OCCs was analyzed under nitrogen. *Comm*-$Na_2C_6O_6$ is stable up to 246 °C, and $Na_4C_6O_6$ shows no obvious weight loss up to 500 °C (Figure S1).

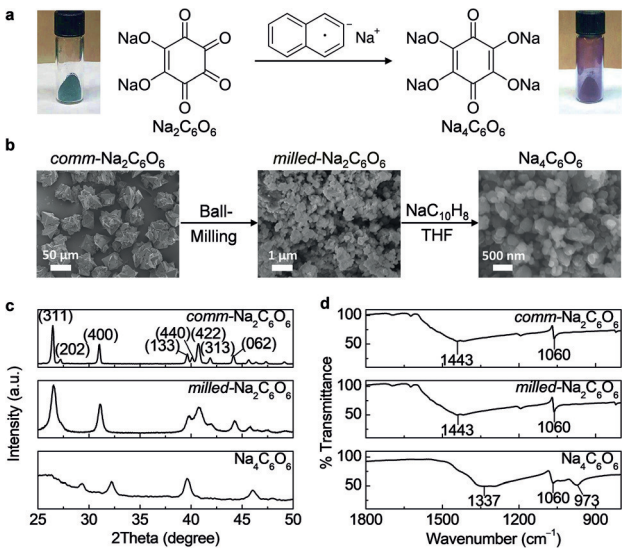

Figure 2. Synthesis and characterization of $Na_4C_6O_6$. a) Chemical reduction/sodiation of $Na_2C_6O_6$ (green powders) into $Na_4C_6O_6$ (purple powders) by reaction with $NaC_{10}H_8$. b) SEM images of pristine $Na_2C_6O_6$, ball-milled $Na_2C_6O_6$, and $Na_4C_6O_6$. c) XRD patterns and d) FT-IR spectra of *comm*-$Na_2C_6O_6$, *milled*-$Na_2C_6O_6$, and $Na_4C_6O_6$, respectively.

The phase structure and purity of the products were confirmed with X-ray diffraction (XRD; Figure 2c). *Milled*-$Na_2C_6O_6$ exhibits the same diffraction peaks as those for *comm*-$Na_2C_6O_6$ (space group *Fddd*).[15] The peak width largely increased confirming the decrease of particle size. After sodiation, the color of powders changed from green to dark purple (Figure 2a). $Na_4C_6O_6$ shows a different diffraction pattern, which coincides with Yamashita's prediction using first-principles calculations that $Na_4C_6O_6$ has a different space group (*C*2/*m*).[15] Although no standard XRD pattern could be used for indexing, four characteristic peaks at 2theta of 29.4°, 32.2°, 39.6°, and 46.0° are the same as those of discharged product of $Na_2C_6O_6$ at 1.6 V, where $Na_4C_6O_6$ formed, in a liquid cell reported by Wang et al.[14] This comparison confirms that our chemically sodiated product is indeed $Na_4C_6O_6$. The change of chemical bond within the molecule was probed by FT-IR spectroscopy (Figure 2d). Pristine and milled $Na_2C_6O_6$ show identical spectra. All the peaks are characteristic of the $C_6O_6^{2-}$ dianions.[16] The sharp peak at 1060 cm^{-1} is assigned to C=C stretching. The broad and strong peak centering at 1443 cm^{-1} represents the vibration of C=O stretching. After sodiation, the broad peak shifts to a smaller wavenumber of 1337 cm^{-1}. Similar shift was observed in the lithiation of $Li_2C_6O_6$ (ca. 1450 cm^{-1})[17] to $Li_4C_6O_6$ (ca. 1400 cm^{-1}),[18] thus confirming successful reduction of $Na_2C_6O_6$. The small peak at 973 cm^{-1} is indicative of a small amount of further reduced C_6O_6 anions,[19] which likely resulted from inhomogeneous reduction.

The sodium-ion conducting SSE, Na_3PS_4, was synthesized through one-step high-energy ball-milling of Na_2S and P_2S_5 without subsequent heat treatment. The XRD pattern and Raman spectrum of only PS_4^{3-} unit in the product (Figure S2) suggest the formation of pure Na_3PS_4 SSE.[10a,20]

The electrochemical properties of Na_3PS_4 and $Na_4C_6O_6$ were measured using pellets sandwiched between ion-blocking electrodes by electrochemical impedance spectroscopy (EIS). $Na_4C_6O_6$ shows no tail in its EIS spectrum, indicating predominant electronic conduction in the material (Figure 3a).[21] Equivalent circuits and fitting results are shown in the inset of Figure 3a and Table S2, respectively. The conductivity of Na_3PS_4 at 60 °C is 3.9×10^{-4} S cm^{-1}, which is comparable to that of Hayashi's Na_3PS_4 prepared through a two-step ball-milling/annealing method.[10a] The conductivity of $Na_4C_6O_6$ is 1.0×10^{-4} S cm^{-1}, which is comparable to that of $LiCoO_2$ and higher than those of $LiMn_2O_4$ and $LiFePO_4$.[22] Calculation from Arrhenius curves shows similar activation energy for $Na_4C_6O_6$ and Na_3PS_4 (Figure 3b). From EIS spectra and polarization curves (Figure S3), we can derive the Na^+ and electron transference numbers for Na_3PS_4 and $Na_4C_6O_6$ as 0.999 and 0.969, respectively. Therefore, Na_3PS_4 is an ionic conductor and $Na_4C_6O_6$ is a mixed electronic-ionic conductor.

We subsequently evaluated the chemical and electrochemical compatibility of Na_3PS_4 with $Na_4C_6O_6$ and its charged form $Na_2C_6O_6$. After mixing and heating Na_3PS_4 with $Na_4C_6O_6$ and $Na_2C_6O_6$, XRD patterns for all materials were unchanged (Figure S4). The S 2p peaks for Na_3PS_4 at 161.9 and 160.7 eV in X-ray photoelectron spectroscopy

 © 2018 Wiley-VCH Verlag GmbH & Co. KGaA, Weinheim

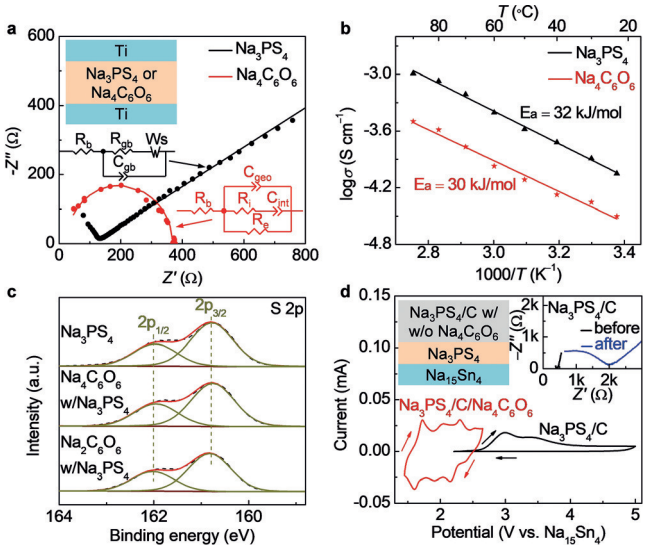

Figure 3. Conductivities of Na_3PS_4 and $Na_4C_6O_6$ and their chemical and electrochemical compatibility. a) EIS spectra of Na_3PS_4 and $Na_4C_6O_6$ pellets at 60 °C sandwiched between ionically blocking electrodes (inset: cell schematic for EIS test and equivalent circuit); b) Arrhenius plot and activation energies of Na_3PS_4 and $Na_4C_6O_6$ conductivities; c) S 2p XPS spectra of pristine Na_3PS_4, $Na_4C_6O_6$/Na_3PS_4 and $Na_2C_6O_6$/Na_3PS_4 mixture after heating at 60 °C; d) Cyclic voltammograms for electrochemical window test of Na_3PS_4 and operating window test of $Na_4C_6O_6$ (left inset: schematic cell set-up for CV test; right inset: electrochemical impedance spectra for Na_3PS_4 cell before and after the CV test). Scan rate: 0.05 mV s^{-1}.

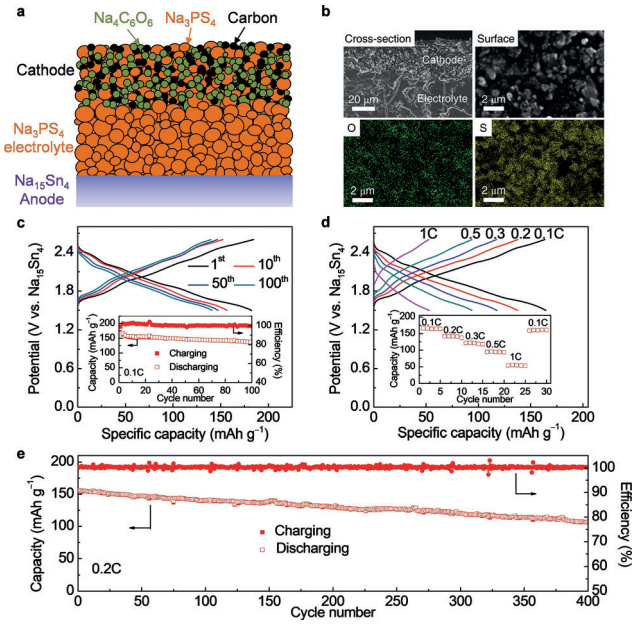

Figure 4. Electrochemical performance of a $Na_4C_6O_6$ | Na_3PS_4 | $Na_{15}Sn_4$ ASSSB. a) Schematic of the ASSSB; b) SEM image of cathode/electrolyte cross-section (left top) and cathode surface (right top) and corresponding EDX mapping of O and S (bottom); c) Charge/discharge voltage profiles at different cycle numbers at 0.1 C at 60 °C (Inset: Capacity and coulombic efficiency versus cycle number at 0.1 C); d) Representative charge/discharge voltage profiles at different current rates (Inset: Rate capabilities and cycling of the battery from 0.1 C to 1 C); e) Capacity and coulombic efficiency versus cycle number at 0.2 C at 60 °C.

(XPS) spectra do not exhibit noticeable change either (Figure 3c),[23] and no signals from oxidized species, for example, polysulfide and S with higher binding energies of >163 eV, were found.[24] Therefore, $Na_4C_6O_6$ is chemically compatible with Na_3PS_4.

Electrochemical compatibility between $Na_4C_6O_6$ and Na_3PS_4 was subsequently investigated by cyclic voltammetry (CV). Na_3PS_4 begins to decompose above 2.6 V versus $Na_{15}Sn_4$ (potential of $Na_{15}Sn_4$ is 0.1 V versus Na^+/Na[25]) and continues to show an irreversible oxidation peak (Figure 3d). EIS spectra show dramatic increase in resistance after the CV scan (inset in Figure 3d), indicating very low ionic conductivities of the decomposition products (e.g. S, P_2S_5 and PS_3^{n-}).[5b] $Na_4C_6O_6$ shows four pairs of redox peaks at 1.60–2.54 V versus $Na_{15}Sn_4$, all below the decomposition potential of Na_3PS_4. Therefore, $Na_4C_6O_6$ and Na_3PS_4 are electrochemically compatible.

The schematic of a $Na_4C_6O_6$ | Na_3PS_4 | $Na_{15}Sn_4$ ASSSB is displayed in Figure 4a. Cold-pressing results in intimate contact between cathode and electrolyte (Figure 4b). The uniformity of the cathode composite (mass ratio of $Na_4C_6O_6$:Na_3PS_4:carbon 4:5:1, active material loading ca. 1 mg cm^{-2}) was examined with energy-dispersive X-ray (EDX) spectroscopy (Figure 4b bottom): O from $Na_4C_6O_6$ is well surrounded by S from Na_3PS_4. The galvanostatic charge/discharge profiles for the ASSSB operated at 0.1 C (1 C = 200 mA g^{-1}) at 60 °C show four distinct voltage plateaus averaging at 2.05 V versus $Na_{15}Sn_4$ (or 2.15 V versus Na^+/Na), reflecting multiple reversible phase transitions between $Na_4C_6O_6$ and $Na_2C_6O_6$ (Figure 4c). With an upper cutoff potential of 2.6 V versus $Na_{15}Sn_4$, $Na_4C_6O_6$ delivers a reversible capacity of 182 mAh g^{-1}, or 90 % of the theoretical capacity, and a 1st-cycle coulombic efficiency as high as 99 %. Charging to even higher potentials is not desirable due to considerable irreversible capacity and significantly increased impedance attributable to the decomposition of Na_3PS_4 (Figure S5). After 100 cycles at 0.1 C and 400 cycles at 0.2 C, the cells deliver charge capacities of 140 and 107 mAh g^{-1}, respectively (Figure 4c,e, and Figure S6). The corresponding capacity retentions are 76 % @100 cycles and 70 % @400 cycles, which are the record cycling performance reported to date for ASSSBs (Table S1). XRD pattern (Figure S4a) and XPS spectrum (Figure S7) of the cycled cathode composite revealed no formation of new species during battery cycling, again proving excellent compatibility between Na_3PS_4 and $Na_4C_6O_6$. The capacity decay may be attributed to the continuous phase transitions between $Na_4C_6O_6$ and $Na_2C_6O_6$[26] as well as the gradual degradation of the SSE–anode interface.[5b]

An ASSSB with $Na_4C_6O_6$ cathode and sodium anode offers a specific energy of up to 395 Wh kg^{-1} at the active-material level, the highest for intercalation compound-based ASSSBs. The battery delivers specific charge capacities of 164, 138, 117, and 94 mAh g^{-1} at cycling rates of 0.1 C, 0.2 C, 0.3 C, and 0.5 C, respectively (Figure 4d).

The above studies concern the cathode performance of $Na_4C_6O_6$ involving two phenolate groups. $Na_4C_6O_6$ also has

© 2018 Wiley-VCH Verlag GmbH & Co. KGaA, Weinheim

two carbonyl groups that can store two additional sodium ions at low potentials through $Na_4C_6O_6 + 2Na^+ + 2e^- \Leftrightarrow Na_6C_6O_6$. Considering the lack of anode materials for ASSSBs besides NaSn alloys, we are motivated to investigate the possibility of $Na_4C_6O_6$ as an anode material. Like the cathode studies, we first examined the chemical compatibility of the fully reduced $Na_6C_6O_6$, also synthesized via chemical reduction (for characterization, see Figures S1 and S8), with Na_3PS_4. XPS spectrum of a heated mixture of the two again revealed sufficient chemical compatibility (Figure S9). The cyclic voltammogram of a $Na_4C_6O_6 | Na_3PS_4 | Na_{15}Sn_4$ battery at low potentials shows only one pair of redox peaks (0.73/1.29 V versus $Na_{15}Sn_4$; Figure S10), in sharp contrast with the multi-peak pattern at high potentials. Correspondingly, discharge profiles show one plateau at ca. 0.8 V versus $Na_{15}Sn_4$ (inset of Figure 5a). $Na_4C_6O_6$ delivers a high specific capacity

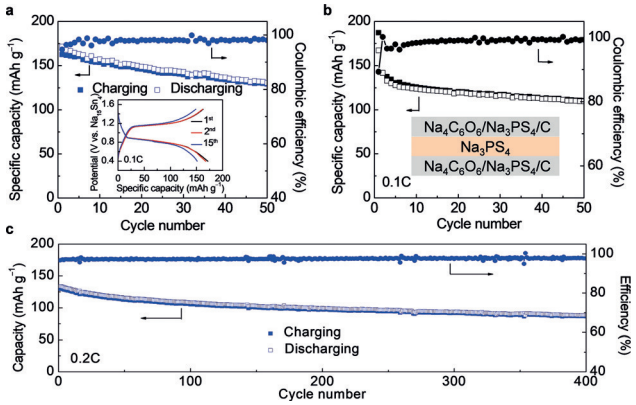

Figure 5. Anode and symmetric full cell performance of $Na_4C_6O_6$ at 60 °C. a) Cycling performance for $Na_4C_6O_6 | Na_3PS_4 | Na_{15}Sn_4$ ASSSB cycled within 0.4–1.5 V (Inset: charge/discharge voltage profile at different cycles); b) Cycling of a symmetric $Na_4C_6O_6 | Na_3PS_4 | Na_4C_6O_6$ full cell (Inset: cell schematic); c) Capacity and coulombic efficiency versus cycle number of $Na_4C_6O_6 | Na_3PS_4 | Na_{15}Sn_4$ ASSSB at 0.2 C.

of 172 mAh g^{-1} at 0.1 C and close to 100 mAh g^{-1} at 0.5 C (Figure S11). Capacity retentions after 50 and 400 cycles at 0.1 and 0.2 C are 77 % and 68 %, respectively (Figure 5a,c and Figure S12). Microcracks are found in the cycled cathode (Figure S13), which may originate from the volumetric change of $Na_4C_6O_6$ during cycling and be responsible for the capacity fading. For comparison, a $Na_4C_6O_6$ battery with an ester-based liquid electrolyte cycled within the same potential range shows only 45 % capacity retention after 15 cycles due to material dissolution (Figure S14). Lee et al.[26] recently reported stable cycling between $Na_2C_6O_6$ and $Na_6C_6O_6$ in an ethereal liquid electrolyte after a high-potential (ca. 3.2 V versus Na^+/Na) activation process, which potential can be detrimental to sulfide SSEs.[5b]

The simultaneous superior cathode and anode performance of $Na_4C_6O_6$ makes a single-material cell feasible. In a symmetric $Na_4C_6O_6 | Na_3PS_4 | Na_4C_6O_6$ cell, the $Na_4C_6O_6$ at the cathode side is desodiated to $Na_2C_6O_6$ during initial charging, while that at the anode side is sodiated to $Na_6C_6O_6$. The reverse process takes place during discharging. The initial discharge/charge capacity of the battery is 167/187 mAh g^{-1} based on the mass of $Na_4C_6O_6$ at the cathode (Figure S15). The symmetric cell shows stable cycling performance with a capacity retention of 66 % after 50 cycles (Figure 5b). The output voltage of the battery is relatively low at ca. 0.65 V, therefore in-serial connection of several unit cells is necessary for higher voltages, which configuration all-solid-state battery uniquely allows for. A single-material cell will simplify cell assembly, reduce cost, and allow for charging in either direction.

In summary, we have successfully developed an organic electrode material ($Na_4C_6O_6$) as both a cathode and an anode material that is chemically and electrochemically compatible with sulfide SSEs. High specific capacity, energy density, and especially stable cycling were demonstrated for $Na_4C_6O_6$-based ASSSBs compared with previously reported ASSSBs. A symmetric all-organic $Na_4C_6O_6$-based ASSSB was finally prototyped.

Acknowledgements

We thank the Solid Sodium team led by Prof. Steve Martin for technical discussion and thank Dr. Zhuan Zhu for assistance in Raman mesurements. Y.Y. acknowledges the funding support from the U.S. Department of Energy's Advanced Research Projects Agency-Energy (ARPA-E) (award number DE-AR0000654) and U.S. Department of Energy's Office of Energy Efficiency and Renewable Energy (EERE), as part of the Battery 500 Consortium (award number DE-EE0008234), and TcSUH.

Conflict of interest

The authors declare no conflict of interest.

Keywords: batteries · carbonyl compounds · energy storage materials · intercalation · organic semiconductors

How to cite: *Angew. Chem. Int. Ed.* **2018**, *57*, 2630–2634
Angew. Chem. **2018**, *130*, 2660–2664

[1] a) J. M. Tarascon, M. Armand, *Nature* **2001**, *414*, 359–367; b) J. G. Kim, B. Son, S. Mukherjee, N. Schuppert, A. Bates, O. Kwon, M. J. Choi, H. Y. Chung, S. Park, *J. Power Sources* **2015**, *282*, 299–322; c) J. Janek, W. G. Zeier, *Nat. Energy* **2016**, *1*, 16141.

[2] a) J.-K. Kim, Y. J. Lim, H. Kim, G.-B. Cho, Y. Kim, *Energy Environ. Sci.* **2015**, *8*, 3589–3596; b) Z. Zhang, Q. Zhang, J. Shi, Y. S. Chu, X. Yu, K. Xu, M. Ge, H. Yan, W. Li, L. Gu, Y.-S. Hu, H. Li, X.-Q. Yang, L. Chen, X. Huang, *Adv. Energy Mater.* **2017**, *7*, 1601196.

[3] a) Y. L. Ni'mah, M.-Y. Cheng, J. H. Cheng, J. Rick, B.-J. Hwang, *J. Power Sources* **2015**, *278*, 375–381; b) C.-W. Park, H.-S. Ryu, K.-W. Kim, J.-H. Ahn, J.-Y. Lee, H.-J. Ahn, *J. Power Sources* **2007**, *165*, 450–454.

[4] a) A. Sakuda, A. Hayashi, M. Tatsumisago, *Sci. Rep.* **2013**, *3*, 2261; b) M. Nose, A. Kato, A. Sakuda, A. Hayashi, M. Tatsumisago, *J. Mater. Chem. A* **2015**, *3*, 22061–22065; c) Z.

 © 2018 Wiley-VCH Verlag GmbH & Co. KGaA, Weinheim

Yu, S.-L. Shang, J.-H. Seo, D. Wang, X. Luo, Q. Huang, S. Chen, J. Lu, X. Li, Z.-K. Liu, D. Wang, *Adv. Mater.* **2017**, *29*, 1605561.
[5] a) I.-H. Chu, C. S. Kompella, H. Nguyen, Z. Zhu, S. Hy, Z. Deng, Y. S. Meng, S. P. Ong, *Sci. Rep.* **2016**, *6*, 33733; b) Y. Tian, T. Shi, W. D. Richards, J. Li, J. C. Kim, S.-H. Bo, G. Ceder, *Energy Environ. Sci.* **2017**, *10*, 1150 – 1166.
[6] A. Banerjee, K. H. Park, J. W. Heo, Y. J. Nam, C. K. Moon, S. M. Oh, S.-T. Hong, Y. S. Jung, *Angew. Chem. Int. Ed.* **2016**, *55*, 9634 – 9638; *Angew. Chem.* **2016**, *128*, 9786 – 9790.
[7] A. Hayashi, K. Noi, N. Tanibata, M. Nagao, M. Tatsumisago, *J. Power Sources* **2014**, *258*, 420 – 423.
[8] a) Y. S. Jung, D. Y. Oh, Y. J. Nam, K. H. Park, *Isr. J. Chem.* **2015**, *55*, 472 – 485; b) N. Ohta, K. Takada, I. Sakaguchi, L. Zhang, R. Ma, K. Fukuda, M. Osada, T. Sasaki, *Electrochem. Commun.* **2007**, *9*, 1486 – 1490; c) S. Yubuchi, Y. Ito, T. Matsuyama, A. Hayashi, M. Tatsumisago, *Solid State Ionics* **2016**, *285*, 79 – 82.
[9] H. Tang, Z. Deng, Z. Lin, Z. Wang, I.-H. Chu, C. Chen, Z. Zhu, C. Zheng, S. P. Ong, *Chem. Mater.* **2018**, *30*, 163 – 173.
[10] a) A. Hayashi, K. Noi, A. Sakuda, M. Tatsumisago, *Nat. Commun.* **2012**, *3*, 856; b) G. H. Newman, L. P. Klemann, *J. Electrochem. Soc.* **1980**, *127*, 2097 – 2099; c) H.-S. Ryu, J.-S. Kim, J.-S. Park, J.-W. Park, K.-W. Kim, J.-H. Ahn, T.-H. Nam, G. Wang, H.-J. Ahn, *J. Electrochem. Soc.* **2013**, *160*, A338 – A343.
[11] a) N. Tanibata, M. Deguchi, A. Hayashi, M. Tatsumisago, *Chem. Mater.* **2017**, *29*, 5232 – 5238; b) J. Yue, F. Han, X. Fan, X. Zhu, Z. Ma, J. Yang, C. Wang, *ACS Nano* **2017**, *11*, 4885 – 4891.
[12] a) Y. Liang, Z. Tao, J. Chen, *Adv. Energy Mater.* **2012**, *2*, 742 – 769; b) Q. Zhao, Y. Lu, J. Chen, *Adv. Energy Mater.* **2017**, *7*, 1601792; c) Y. Liang, Y. Jing, S. Gheytani, K.-Y. Lee, P. Liu, A. Facchetti, Y. Yao, *Nat. Mater.* **2017**, *16*, 841 – 848; d) Y. Jing, Y. Liang, S. Gheytani, Y. Yao, *Nano Energy* **2017**, *37*, 46 – 52; e) Q. Zhao, Z. Zhu, J. Chen, *Adv. Mater.* **2017**, *29*, 1607007; f) K. Chihara, N. Chujo, A. Kitajou, S. Okada, *Electrochim. Acta* **2013**, *110*, 240 – 246; X. Wu, S. Jin, Z. Zhang, L. Jiang, L. Mu, Y.-S. Hu, H. Li, X. Chen, M. Armand, L. Chen, X. Huang, *Sci. Adv.* **2015**, *1*, e1500330; H. Kim, D.-H. Seo, G. Yoon, W. A. Goddard, Y. S. Lee, W.-S. Yoon, K. Kang, *J. Phys. Chem. Lett.* **2014**, *5*, 3086 – 3092.
[13] B. Häupler, A. Wild, U. S. Schubert, *Adv. Energy Mater.* **2015**, *5*, 1402034.
[14] Y. Wang, Y. Ding, L. Pan, Y. Shi, Z. Yue, Y. Shi, G. Yu, *Nano Lett.* **2016**, *16*, 3329 – 3334.
[15] T. Yamashita, H. Momida, T. Oguchi, *J. Phys. Soc. Jpn.* **2015**, *84*, 074703.
[16] R. T. Bailey, *J. Chem. Soc. B* **1971**, 627 – 629.
[17] H. Chen, M. Armand, G. Demailly, F. Dolhem, P. Poizot, J.-M. Tarascon, *ChemSusChem* **2008**, *1*, 348 – 355.
[18] H. Chen, M. Armand, M. Courty, M. Jiang, C. P. Grey, F. Dolhem, J.-M. Tarascon, P. Poizot, *J. Am. Chem. Soc.* **2009**, *131*, 8984 – 8988.
[19] J.-C. Guo, H.-G. Lu, S.-D. Li, *Comput. Theor. Chem.* **2013**, *1018*, 95 – 101.
[20] Y. So, H. Akitoshi, T. Masahiro, *Chem. Lett.* **2015**, *44*, 884 – 886.
[21] R. A. Huggins, *Ionics* **2002**, *8*, 300 – 313.
[22] M. Park, X. Zhang, M. Chung, G. B. Less, A. M. Sastry, *J. Power Sources* **2010**, *195*, 7904 – 7929.
[23] S. Wenzel, T. Leichtweiss, D. A. Weber, J. Sann, W. G. Zeier, J. Janek, *ACS Appl. Mater. Interfaces* **2016**, *8*, 28216 – 28224.
[24] R. Koerver, I. Aygün, T. Leichtweiß, C. Dietrich, W. Zhang, J. O. Binder, P. Hartmann, W. G. Zeier, J. Janek, *Chem. Mater.* **2017**, *29*, 5574 – 5582.
[25] V. L. Chevrier, G. Ceder, *J. Electrochem. Soc.* **2011**, *158*, A1011 – A1014.
[26] M. Lee, J. Hong, J. Lopez, Y. Sun, D. Feng, K. Lim, W. C. Chueh, M. F. Toney, Y. Cui, Z. Bao, *Nat. Energy* **2017**, *2*, 861 – 868.

Manuscript received: December 14, 2017
Accepted manuscript online: January 24, 2018
Version of record online: February 8, 2018

 © 2018 Wiley-VCH Verlag GmbH & Co. KGaA, Weinheim